

Electronic Supplementary Information

Experimental Section

Materials: Sodium carbonate (Na_2CO_3 , 99.0%), hydrochloric acid (HCl, 99.0%), ammonium chloride (NH_4Cl), ethanol ($\text{C}_2\text{H}_6\text{O}$, 99.0%), salicylic acid ($\text{C}_7\text{H}_6\text{O}_3$), sodium citrate dehydrate ($\text{C}_6\text{H}_5\text{Na}_3\text{O}_7 \cdot 2\text{H}_2\text{O}$), *p*-dimethylaminobenzaldehyde ($\text{C}_9\text{H}_{11}\text{NO}$), sodium nitroferricyanide dihydrate ($\text{C}_5\text{FeN}_6\text{Na}_2\text{O} \cdot 2\text{H}_2\text{O}$) and sodium hypochlorite solution (NaClO) were purchased from Aladdin Ltd. (Shanghai, China). Nafion (5 wt%) solution was purchased from Sigma-Aldrich Chemical Reagent Co., Ltd. Nitric acid (HNO_3), sulfuric acid (H_2SO_4), hydrogen peroxide (H_2O_2), hydrazine monohydrate ($\text{N}_2\text{H}_4 \cdot \text{H}_2\text{O}$) and ethyl alcohol ($\text{C}_2\text{H}_5\text{OH}$) were purchased from Beijing Chemical Corp. (China). chemical Ltd. in Chengdu. The ultrapure water used throughout all experiments was purified through a Millipore system. All reagents were analytical reagent grade without further purification.

Preparation of $\text{Mo}_3\text{Si}/\text{GP}$: The in situ growth of the Mo_3Si thin film on graphite paper (GP) substrate was carried out via a direct current magnetron sputtering system. The GP was cleaned using acetone and ethanol for 5 min in an ultrasonic bath, followed by rinsing with deionized water. Prior to film preparation, the sputter chamber was evacuated to approximately 10^{-4} Pa. The distance between the target and GP substrate was about 120 mm. Argon gas (30 sccm, purity: 99.999%) was introduced into chamber with total pressure of 3 Pa and the sputtering power was controlled at 370 W. The growth time on GP were 30 min. The samples were obtained as $\text{Mo}_3\text{Si}/\text{GP}$.

Characterizations: Power XRD data were acquired by a LabX XRD-6100 X-ray diffractometer with a $\text{Cu K}\alpha$ radiation (40 kV, 30 mA) of wavelength 0.154 nm (SHIMADZU, Japan). SEM images were collected on a GeminiSEM 300 scanning electron microscope (ZEISS, Germany) at an accelerating voltage of 5 kV. TEM images were acquired on a HITACHI H-8100 electron microscopy (Hitachi, Tokyo, Japan) operated at 200 kV. XPS measurements were performed on an ESCALABMK II X-ray photoelectron spectrometer using Mg as the exciting source. The absorbance data of spectrophotometer was measured on UV-Vis spectrophotometer. The ion chromatography data were collected on Metrohm 940 Professional IC Vario.

Electrochemical measurements: In this paper, we use a H-type electrolytic cell separated by a Nafion 117 Membrane which was protonated by boiling in ultrapure water, H_2O_2 (5%) aqueous solution and 0.5 M H_2SO_4 at 80 °C for another 2 h, respectively. A three-electrode configuration is used for electrochemical experiments which the catalyst of Mo_3Si thin film

on graphite paper substrate as the working electrode, the Ag/AgCl/saturated KCl is the reference electrode and graphite rod as the counter electrode. The electrochemical experiments were carried out with an electrochemical workstation (CHI 660E) in N₂-saturated 0.1 M Na₂SO₄ solution. The potentials reported in this work were converted to reversible hydrogen electrode (RHE) scale via calibration with the following equation: E (RHE) = E (vs. Ag/AgCl) + 0.61 V and the presented current density was normalized to the geometric surface area.

Determination of NH₃: Concentration of produced NH₃ was determined by spectrophotometry measurement with indophenol blue method.¹ In detail, 4 mL electrolyte was obtained from the cathodic chamber and mixed with 50 μL oxidizing solution containing NaClO (4.5%) and NaOH (0.75 M), 500 μL coloring solution containing C₇H₅O₃Na (0.4 M) and NaOH (0.32 M), and 50 μL catalyst solution Na₂Fe(CN)₅NO·2H₂O (1 wt%) for 1 h. The concentration-absorbance curve was calibrated using the standard NH₄Cl solution with NH₃ concentrations of 0.0, 0.05, 0.10, 0.15, 0.20, 0.3, 0.4 and 0.6 μg mL⁻¹ in 0.1 M Na₂SO₄. These solutions were identified via UV-Vis spectroscopy at the wavelength of 655 nm. The concentration-absorbance curve was calibrated using standard NH₃ solution with a series of concentrations. The fitting curve ($y = 0.56x + 0.02$, $R^2 = 0.999$) shows good linear relation of absorbance value with NH₃ concentration.

Determination of N₂H₄: The N₂H₄ production was estimated by the method of Watt and Chrisp.² The color reagent was a mixed solution of 5.99 g C₉H₁₁NO, 30 mL HCl and 300 mL C₂H₅OH. In detail, 5 mL electrolyte was removed from the electrochemical reaction vessel, and added into 5 mL prepared color reagent and stirred 15 min at 25 °C. The absorbance of such solution at the absorbance of 455 nm was measured to quantify the hydrazine yields with a standard curve of hydrazine ($y = 0.64x + 0.084$, $R^2 = 0.998$).

Determination of FE and NH₃ yield: The FE was calculated by equation:

$$FE = 3 \times F \times [\text{NH}_3] \times V / 17 \times Q \times 100\%$$

NH₃ yield was calculated using the following equation:

$$\text{NH}_3 \text{ yield} = [\text{NH}_3] \times V / (17 \times t \times A)$$

The amount of NH₃ was calculated as follows:

$$m_{\text{NH}_3} = [\text{NH}_3] \times V$$

Where F is the Faraday constant (96500 C mol⁻¹), [NH₃] is the measured NH₃ concentration, V is the volume of the cathodic reaction electrolyte, Q is the total quantity of applied electricity; t is the reduction time (2h) and A is the loaded area of catalyst.

Computational details:

Density functional theory (DFT) calculations were performed by using the Vienna ab initio simulation package (VASP) with the projected augment wave (PAW) pseudopotential^{3,4} and the Perdew, Burke, and Ernzerhof (PBE) functional.⁵ The DFT+D3 method has been adopted to describe the van der Waals interactions.⁶ The convergence criteria for the total energy and the Hellmann-Feynman force were 10^{-5} eV and $0.02 \text{ eV}\text{\AA}^{-1}$, respectively. The Mo_3Si (210) (2×1) supercell was adopted with a vacuum layer of $\sim 15 \text{ \AA}$ for modelling the nitrogen reduction reaction. For such supercell, $3\times 2\times 1$ Monkhorst-Pack grid⁷ was used with the kinetic cutoff energy of 450 eV for the plane-wave basis set. The calculations of the Gibbs free-energy change for elemental steps have adopted the computational hydrogen electrode model,⁸ which can be obtained by the following equation

$$\Delta G = \Delta E + \Delta E_{\text{ZPE}} - T\Delta S$$

The total energy (E), zero-point energy (E_{ZPE}), and entropy (S) of the adsorbed intermediates were obtained from DFT calculations (Tables S2 and S3), while the thermodynamic corrections of the free molecules taken from the NIST databases.⁹

The adsorption energies (E_a) of N_2 molecules and H atoms were calculated according to the equation $E_a = E_{\text{support}} + E_{\text{mol}} - E_{\text{tot}}$, where E_{mol} is referred to the total energy of the free molecule, and E_{support} and E_{tot} are the total energies of the bare support and that with the adsorbate, respectively.

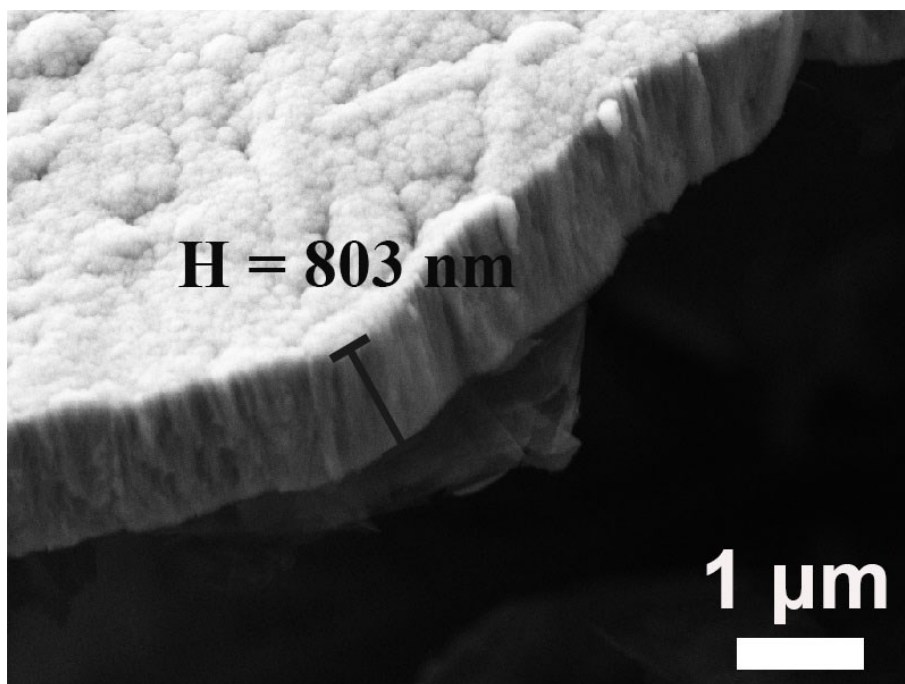


Fig. S1. Cross-section SEM image of Mo₃Si.

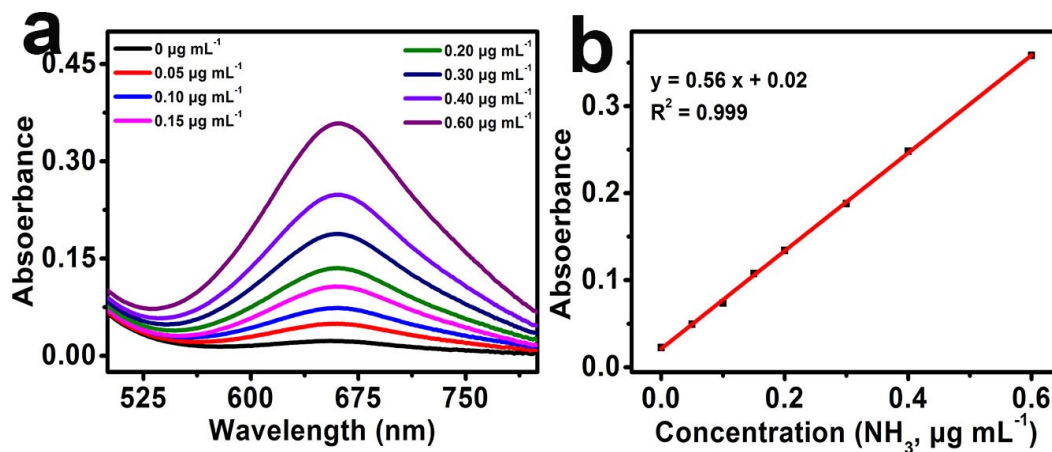


Fig. S2. (a) UV-Vis absorption curves of indophenol assays kept with different concentrations of NH_4^+ ions for 1 h at room temperature. (b) A calibration curve used to estimate the concentration of NH_3 concentration.

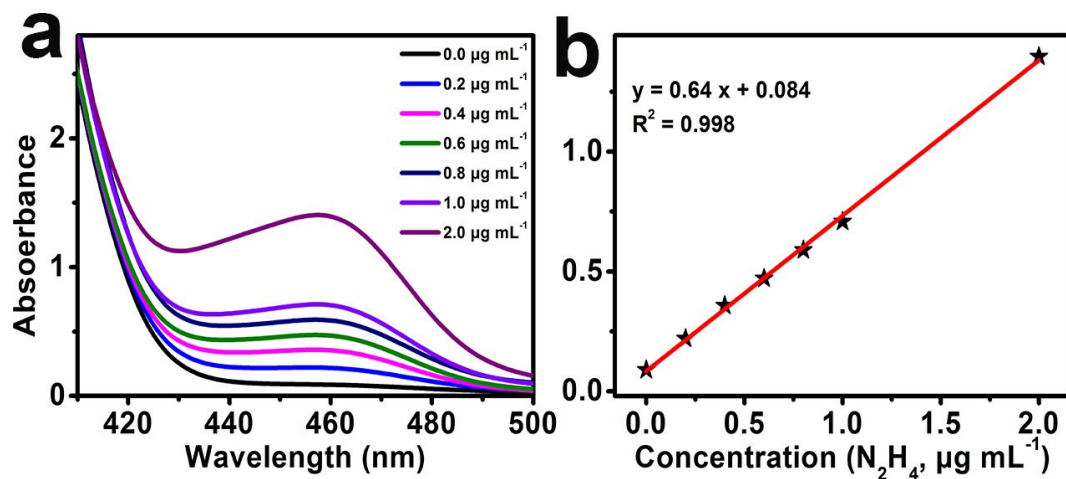


Fig. S3. (a) UV-Vis curves of various N_2H_4 concentrations after incubated for 15 min at room temperature. (b) Calibration curve used for calculation of N_2H_4 concentrations.

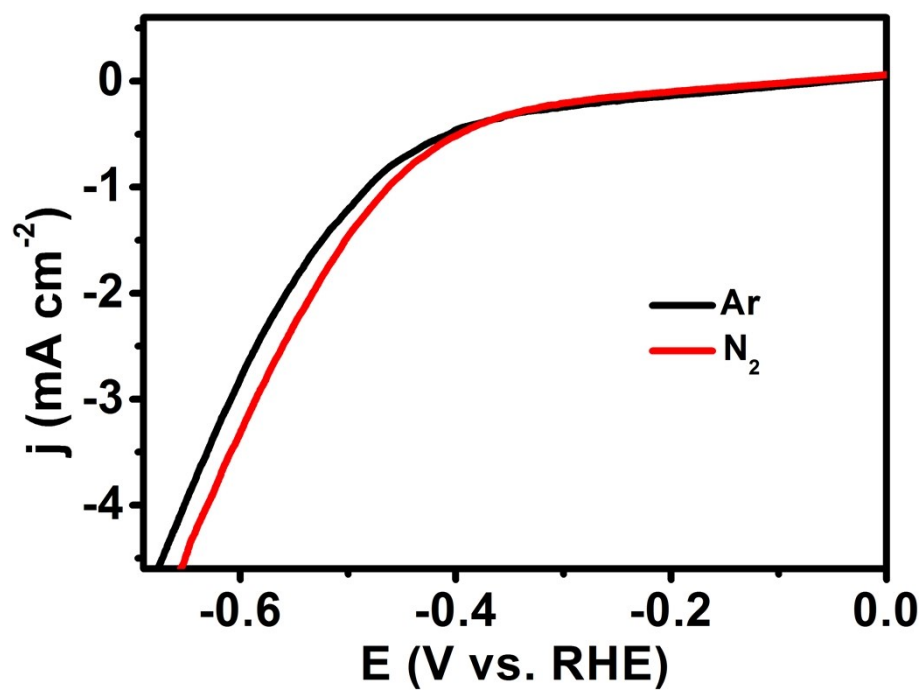


Fig. S4. Linear sweep voltammetry curves of Mo₃Si/GP in Ar- and N₂-saturated 0.1 M Na₂SO₄.

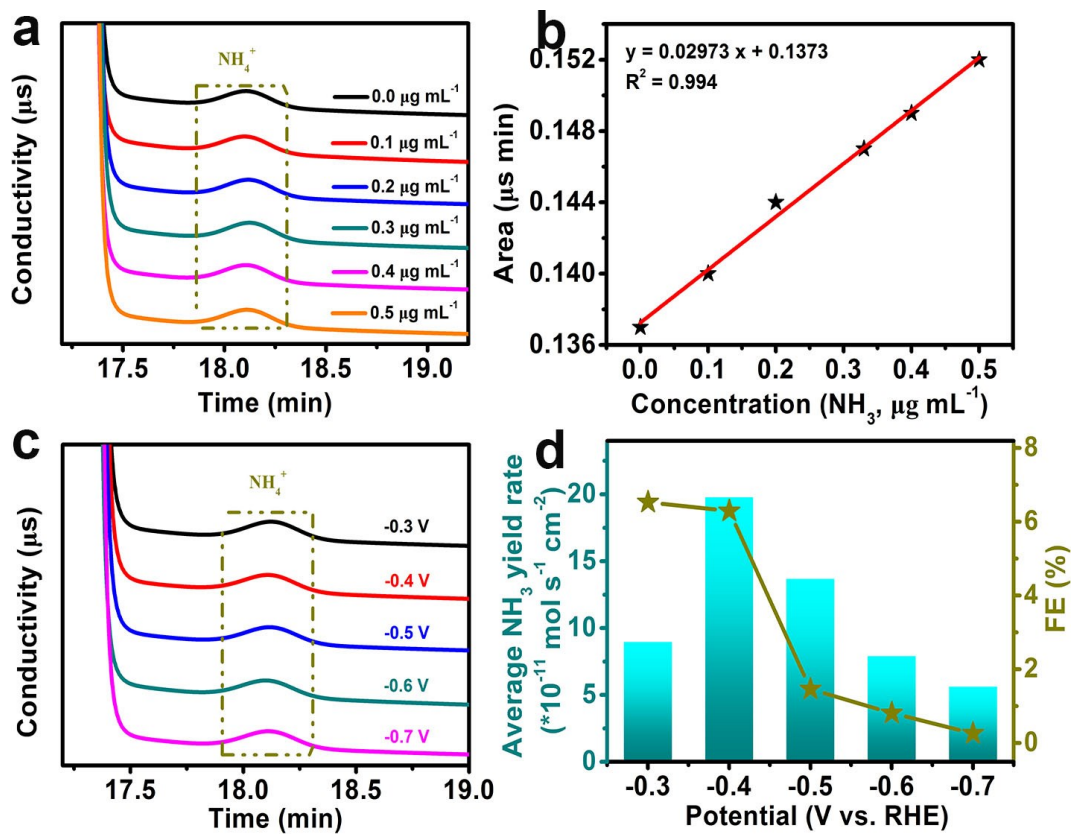


Fig. S5. (a) Ion chromatogram of NH_4Cl with different concentrations in 0.1 M Na_2SO_4 and (b) Corresponding standard curve. (c) Ion chromatogram for the electrolytes at a series of potentials after electrolysis for 2 h. (d) NH_3 yields and FEs of $\text{Mo}_3\text{Si/GP}$ at corresponding potentials.

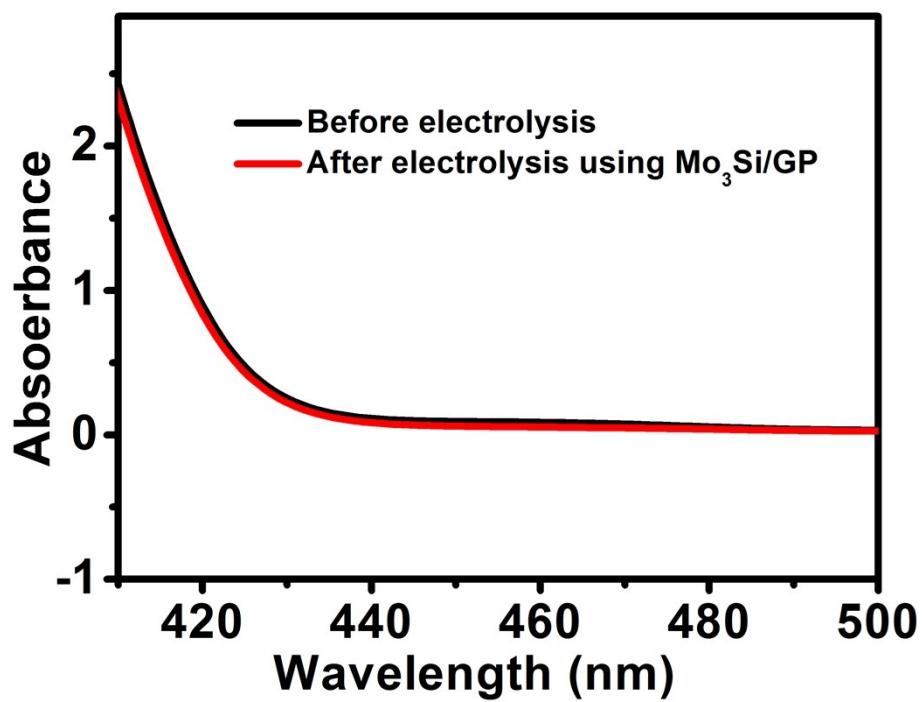


Fig. S6. UV-Vis absorption spectra of the electrolytes estimated by the method of Watt and Chrisp before and after 2 h electrolysis in N₂ atmosphere at -0.4 V.

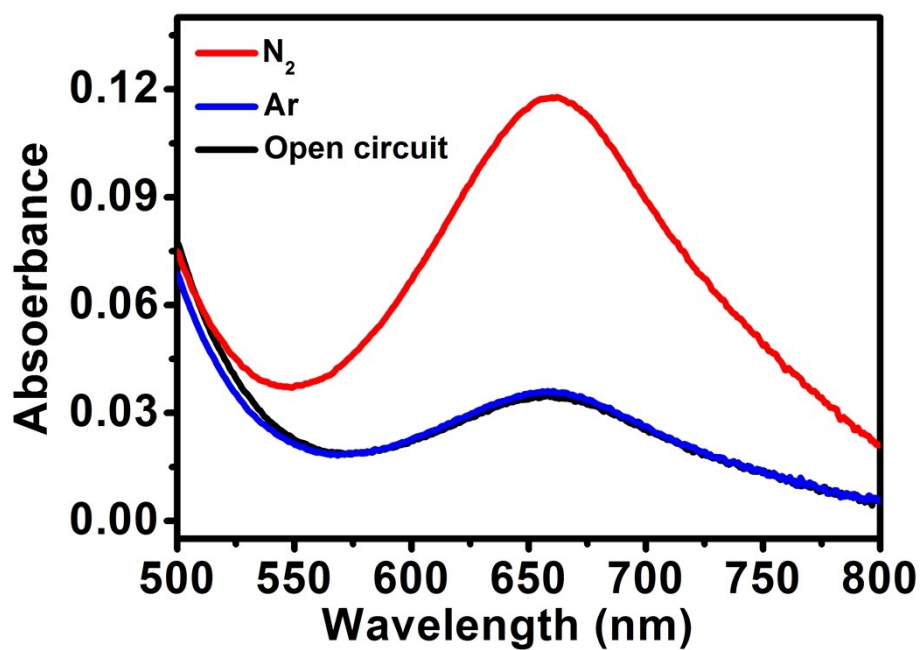


Fig. S7. UV-Vis absorption spectra of the electrolytes colored with indophenol indicator after 2 h electrolysis under different conditions.

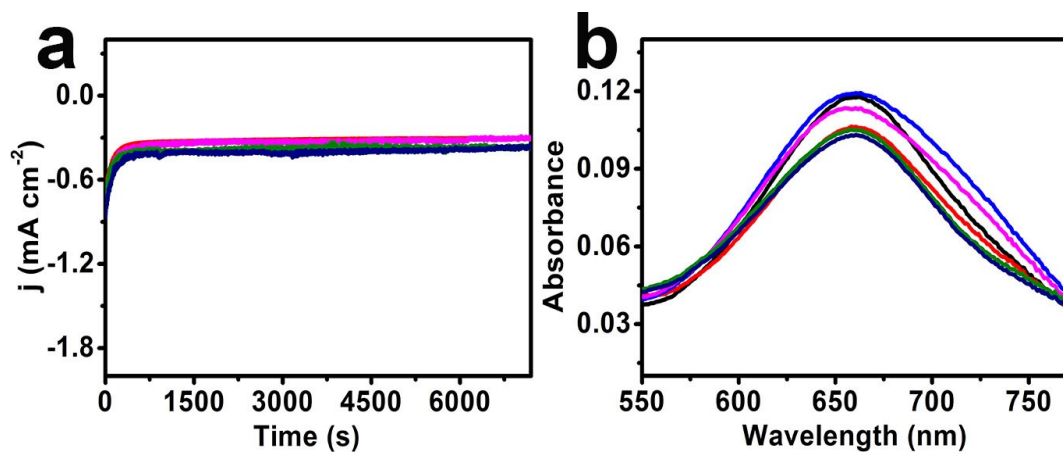


Fig. S8. (a) Time-dependent current density curves of Mo₃Si/GP under recycling tests for NRR at -0.4 V in 0.1 M Na₂SO₄. (b) UV-Vis absorption spectra of the electrolytes stained with indophenol indicator after NRR electrolysis.

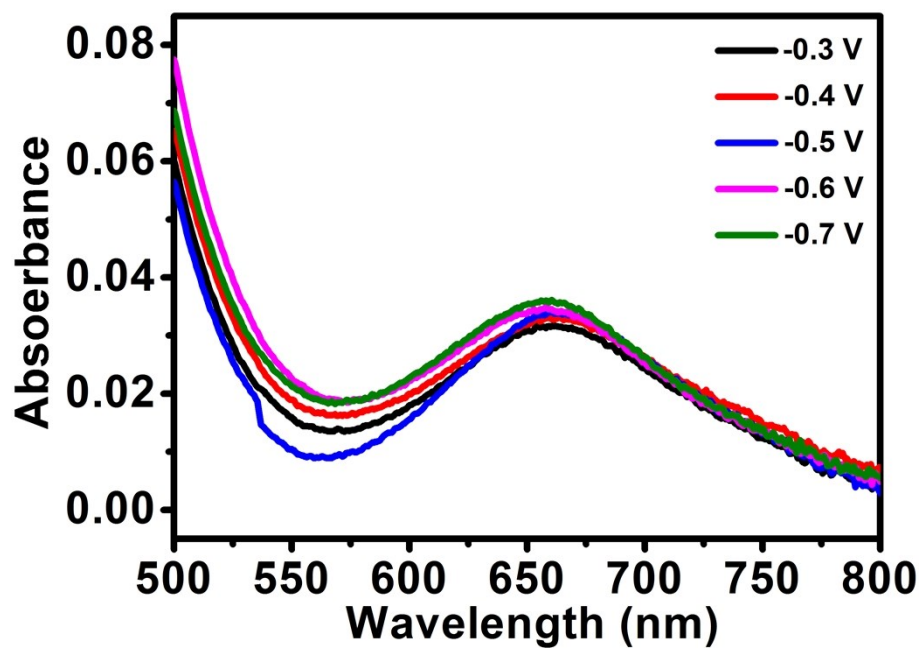


Fig. S9. UV-Vis absorption spectra of the anodic electrolytes colored with indophenol indicator.

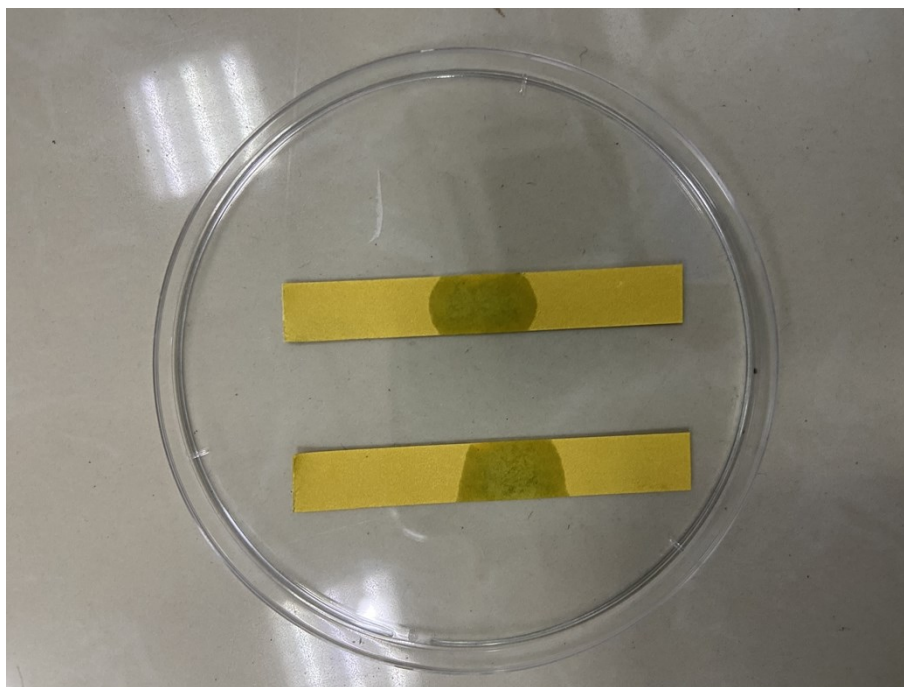


Fig. S10. Photographs of pH test papers in 0.1 M Na_2SO_4 before and after 2 h electrolysis.

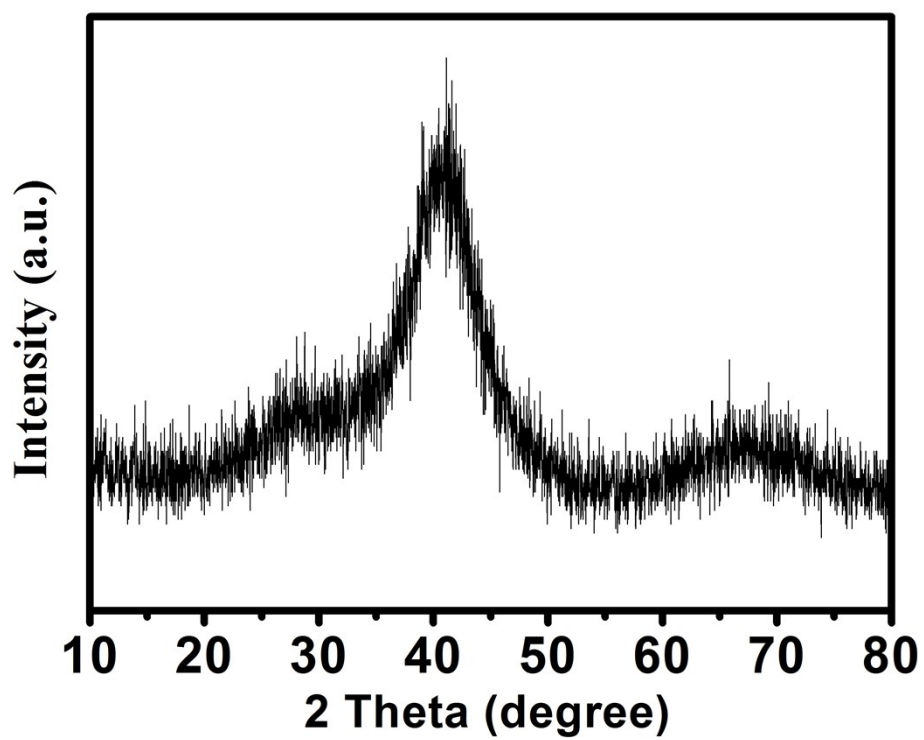


Fig. S11. XRD pattern for Mo₃Si/GP after stability test.

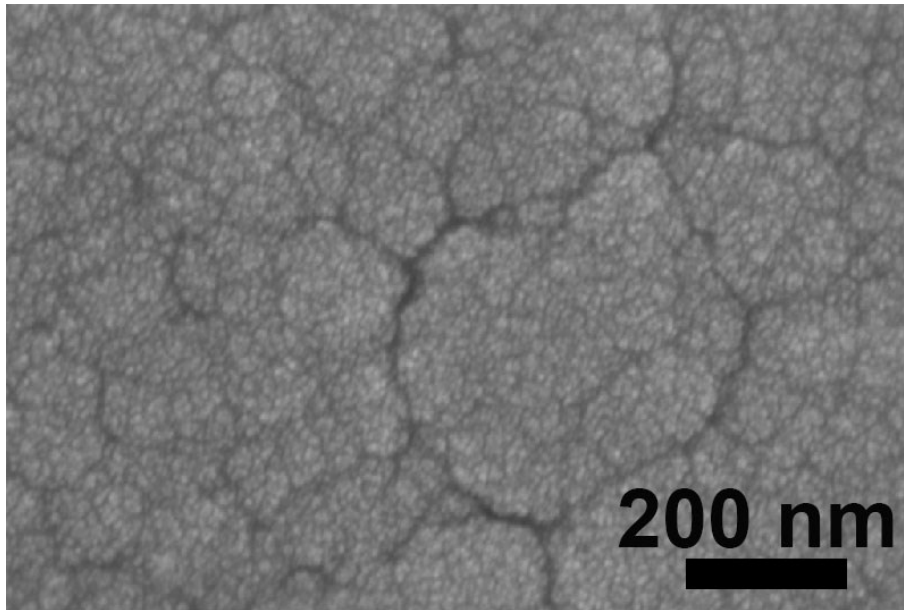


Fig. S12. SEM image of Mo₃Si/GP after stability test.

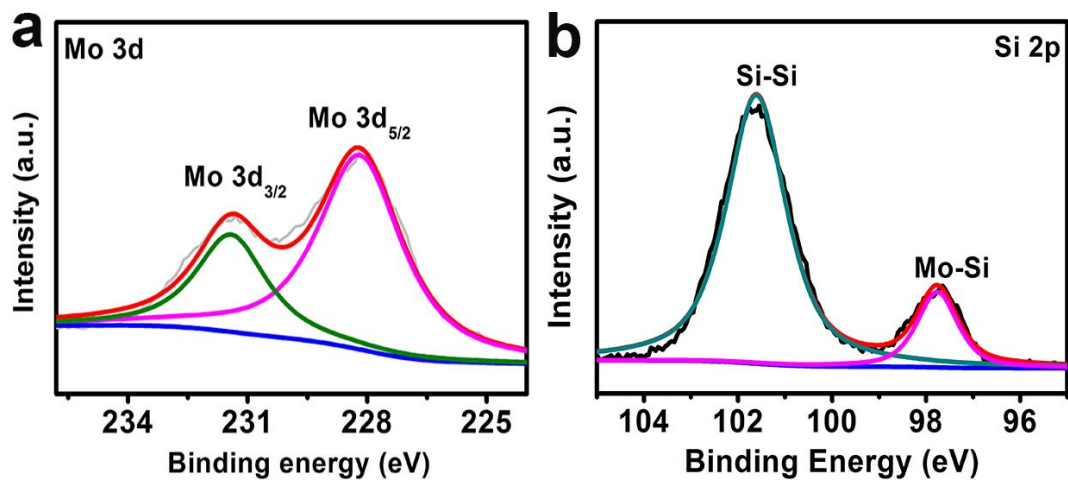


Fig. S13. XPS spectra in the (a) Mo 3d and (b) Si 2p regions for Mo₃Si after stability test.

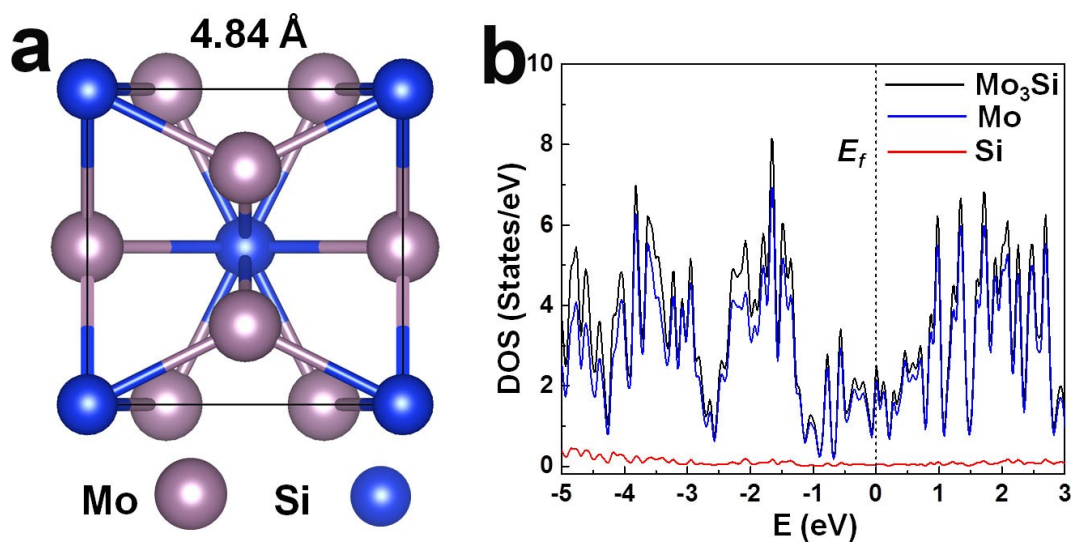


Fig. S14. Unit cell and the densities of states (DOS) of Mo₃Si. For DOS, the total DOS of Mo₃Si, and the local DOS projected on the Mo and Si atoms are presented. The dashed line denotes the position of Fermi level (E_f).

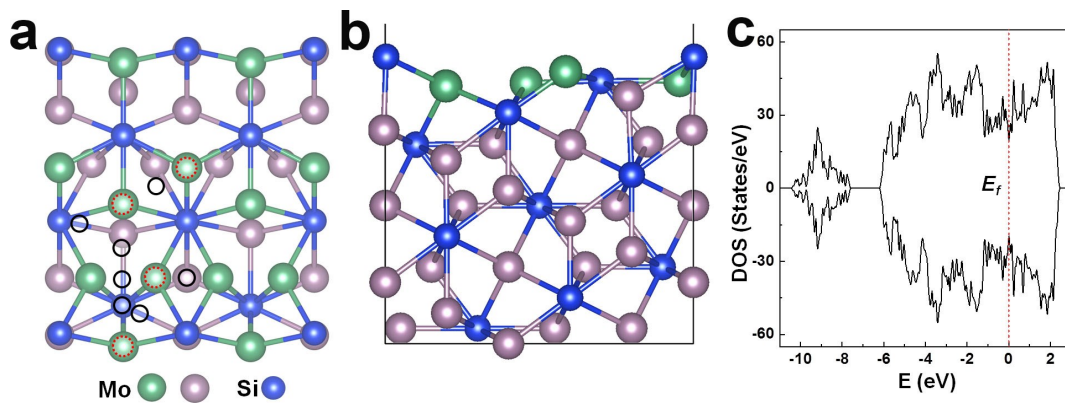


Fig. S15. Top (a) and side (b) views of the Mo₃Si (210) (2×1) surface. The slab model contains five repeated units, in which the bottom three ones are fixed to mimic the bulk. The total DOS of the Mo₃Si (210) (2×1) surface are displayed in (c), where the dashed line denotes the position of Fermi level (E_f). In (a), the rough adsorption sites for N₂ molecules are marked by the dotted (the top site) and solid (the bridge and hollow sites) circles. In (a), for clarity, only the first several atomic layers are displayed, and the Mo atom exposed are denoted as deep green spheres.

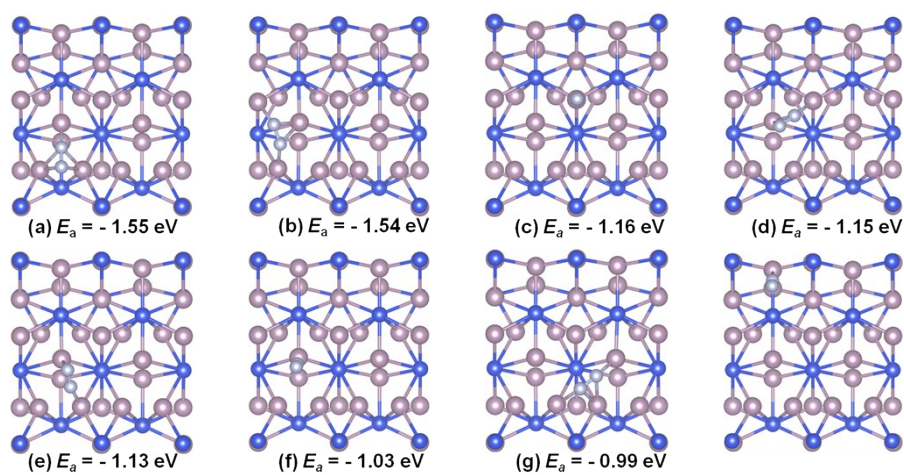


Fig. S16. Top views of the various optimized configurations for the N_2 adsorption on the sites shown in Fig. S15a. The adsorption energies (E_a in eV) are given. The small grey spheres denote the N atoms. The configurations in (a) and (b) are referred to as N_2^α and N_2^β , respectively.

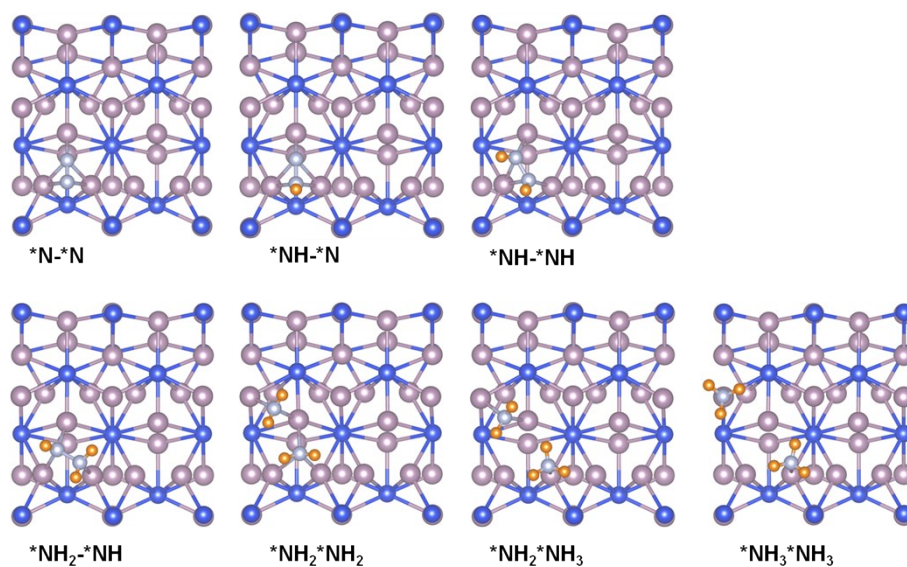


Fig. S17. Local atomic structures of the reaction intermediates for the NRR, presented in Fig. 4a, on the Mo₃Si (210) (2×1) surface. The small yellow spheres denote the H atoms.

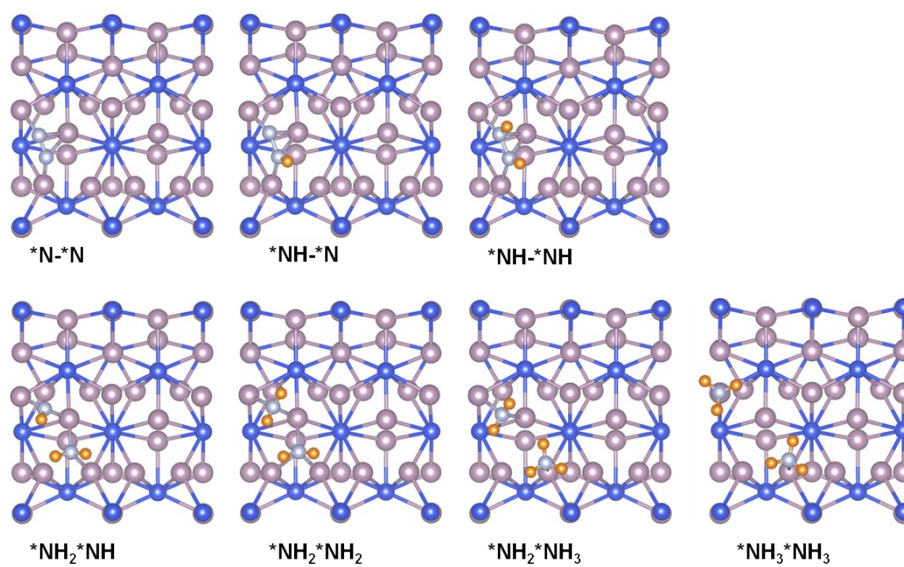


Fig. S18. Local atomic structures of the reaction intermediates for the NRR, presented in Fig. 4b, on the Mo₃Si (210) (2×1) surface.

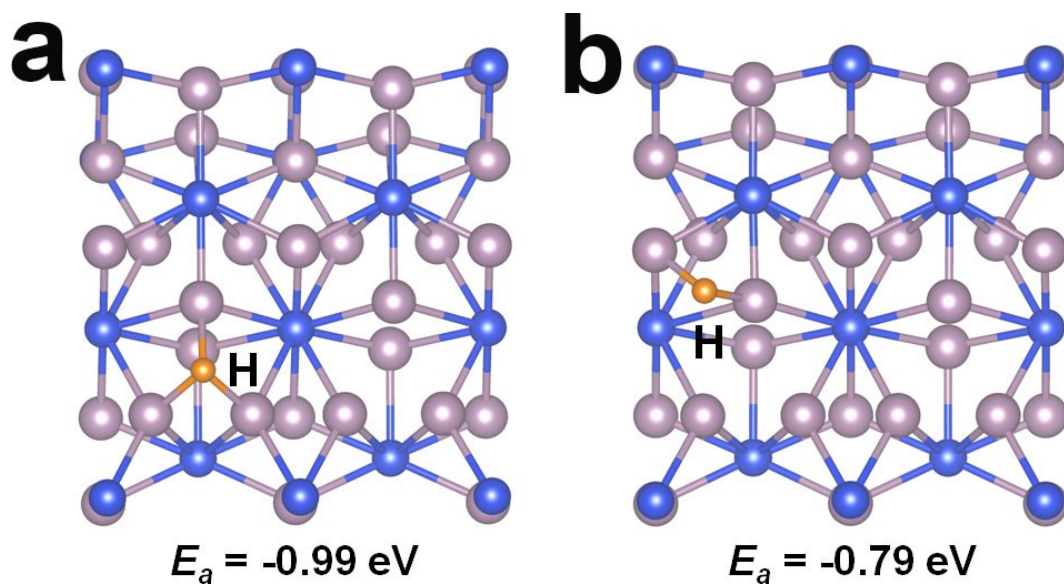


Fig. S19. Top views of the configurations for the H adsorption on the two selected sites. The adsorption energies (E_a in eV) are given.

Table S1. Comparison of electrocatalytic NRR performance for Mo₃Si with other electrocatalysts under ambient conditions.

Catalyst	Electrolyte	NH ₃ yield	FE (%)	Ref.
Mo ₃ Si	0.1 M Na ₂ SO ₄	$2 \times 10^{-10} \text{ mol s}^{-1} \text{ cm}^{-2}$	6.69	This work
		$12.24 \times 10^{-10} \mu\text{g h}^{-1} \text{ cm}^{-2}$		
		$30.6 \mu\text{g h}^{-1} \text{ mg}^{-1}_{\text{cat.}}$		
MoS ₂	0.1 M Na ₂ SO ₄	$8.08 \times 10^{-11} \text{ mol s}^{-1} \text{ cm}^{-2}$	1.17	10
Mo nanofilm	0.01 M H ₂ SO ₄	$3.09 \times 10^{-11} \text{ mol s}^{-1} \text{ cm}^{-2}$	0.72	11
Co-dopd MoS _{2-x}	0.01 M H ₂ SO ₄	$0.6 \text{ mmol h}^{-1} \text{ mg}^{-1}_{\text{cat.}}$	10	12
Mo ₂ C	0.5 M Li ₂ SO ₄	$11.3 \mu\text{g h}^{-1} \text{ mg}^{-1}_{\text{cat.}}$	7.8	13
MoN	0.1 M HCl	$3.01 \times 10^{-10} \text{ mol s}^{-1} \text{ cm}^{-2}$	1.15	14
Mo ₂ N	0.1 M HCl	$4.6 \times 10^{-10} \text{ mol s}^{-1} \text{ cm}^{-2}$	4.5	15
MoO ₃	0.1 M HCl	$4.8 \times 10^{-10} \text{ mol s}^{-1} \text{ cm}^{-2}$	1.9	16
Bi ₂ MoO ₆	0.1 M HCl	$1.6 \times 10^{-10} \text{ mol s}^{-1} \text{ cm}^{-2}$	8.17	17
MnO ₂ with oxygen vacancies	0.1 M Na ₂ SO ₄	$1.63 \times 10^{-10} \text{ mol s}^{-1} \text{ cm}^{-2}$	11.40	18
Ti ³⁺ -TiO _{2-x}	0.1 M Na ₂ SO ₄	$3.51 \times 10^{-11} \text{ mol s}^{-1} \text{ cm}^{-2}$	14.62	19
porous bromide-derived Ag film	0.1 M Na ₂ SO ₄	$2.07 \times 10^{-11} \text{ mol s}^{-1} \text{ cm}^{-2}$	7.36	20
Bi nanosheet array	0.1 M HCl	$6.89 \times 10^{-11} \text{ mol s}^{-1} \text{ cm}^{-2}$	10.26	21
d-TiO ₂	0.1 M HCl	$1.24 \times 10^{-10} \text{ mol s}^{-1} \text{ cm}^{-2}$	9.17	22
VN	0.1 M HCl	$8.40 \times 10^{-11} \text{ mol s}^{-1} \text{ cm}^{-2}$	2.25	23
N-C@NiO	0.1 M HCl	$8.09 \mu\text{g h}^{-1} \text{ mg}^{-1}_{\text{cat.}}$	11.59	24
Bi ₄ V ₂ O ₁₁ /CeO ₂	0.1 M HCl	$23.21 \mu\text{g h}^{-1} \text{ mg}^{-1}_{\text{cat.}}$	10.16	25

Table S2. The calculated zero-point energy (E_{ZPE}) and the product (TS) of temperature ($T = 298.15$ K) and entropy (S) of the different species along the reaction pathway presented in Fig. 4a, where * represents the adsorption site.

Species	E_{ZPE} (eV)	TS (eV)
N ₂	0.15	0.58
*N-*N	0.20	0.08
*NH-*N	0.51	0.09
*NH-*NH	0.84	0.09
*NH ₂ -*NH	1.18	0.11
*NH ₂ *NH ₂	1.37	0.15
*NH ₂ *NH ₃	1.72	0.21
*NH ₃ *NH ₃	2.03	0.31
1/2H ₂	0.14	0.21
NH ₃	0.89	0.60

Table S3. Similar to Table S2, except that it is for the he reaction pathway presented in Fig. 4b.

Species	E_{ZPE} (eV)	TS (eV)
N ₂	0.15	0.58
*N-*N	0.19	0.08
*NH-*N	0.52	0.08
*NH-*NH	0.84	0.09
*NH ₂ *NH	1.03	0.14
*NH ₂ *NH ₂	1.37	0.15
*NH ₂ *NH ₃	1.72	0.21
*NH ₃ *NH ₃	2.03	0.31
1/2H ₂	0.14	0.21
NH ₃	0.89	0.60

References

- 1 D. Zhu, L. Zhang, R. E. Ruther and R. J. Hamers, *Nat. Mater.*, 2013, **12**, 836–841.
- 2 G. W. Watt and J. D. Chrisp, *Anal. Chem.*, 1952, **24**, 2006–2008.
- 3 P. E. Blöchl, *Phys. Rev. B*, 1994, **50**, 17953–17979.
- 4 G. Kresse and J. Furthmüller, *Phys. Rev. B*, 1996, **54**, 11169.
- 5 J. P. Perdew, K. Burke and M. Ernzerhof, *Phys. Rev. Lett.*, 1996, **77**, 3865–3868.
- 6 S. Grimme, J. Antony, S. Ehrlich and H. Krieg, *J. Chem. Phys.*, 2010, **132**, 154104.
- 7 H. J. Monkhorst and J. D. Pack, *Phys. Rev. B*, 1976, **13**, 5188–5192.
- 8 J. K. Nørskov, J. Rossmeisl, A. Logadottir, L. Lindqvist, J. R. Kitchin, T. Bligaard and H. Jónsson, *J. Phys. Chem. B*, 2004, **108**, 17886–17892.
- 9 <http://webbook.nist.gov/chemistry/>.
- 10 L. Zhang, X. Ji, X. Ren, Y. Ma, X. Shi, Z. Tian, A. M. Asiri, L. Chen, B. Tang and X. Sun, *Adv. Mater.*, 2018, **30**, 201800191.
- 11 D. Yang, T. Chen and Z. Wang, *J. Mater. Chem. A*, 2017, **5**, 18967–18971.
- 12 J. Zhang, X. Tian, M. Liu, H. Guo, J. Zhou, Q. Fang, Z. Liu, Q. Wu and J. Lou, *J. Am. Chem. Soc.*, 2019, **141**, 19269–19275.
- 13 H. Cheng, L. Ding, G. Chen, L. Zhang, J. Xue and H. Wang, *Adv. Mater.* 2018, **30**, 1803694.
- 14 L. Zhang, X. Ji, X. Ren, Y. Luo, X. Shi, A. M. Asiri, B. Zheng and X. Sun, *ACS Sustainable Chem. Eng.*, 2018, **6**, 9550–9554.
- 15 X. Ren, G. Cui, L. Chen, F. Xie, Q. Wei, Z. Tian and X. Sun, *Chem. Commun.*, 2018, **54**, 8474–8477.
- 16 J. Han, X. Ji, X. Ren, G. Cui, L. Li, F. Xie, H. Wang, B. Li and X. Sun, *J. Mater. Chem. A*, 2018, **6**, 12974.
- 17 Z. Xing, W. Kong, T. Wu, H. Xie, T. Wang, Y. Luo, X. Shi, A. M. Asiri, Y. Zhang and X. Sun, *ACS Sustainable Chem. Eng.*, 2019, **7**, 12692–12696.
- 18 Y. Zhang, H. Du, Y. Ma, L. Ji, H. Guo, Z. Tian, H. Chen, H. Huang, G. Cui, A. M. Asiri, F. Qu, L. Chen and X. Sun, *Nano Res.*, 2019, **12**, 919–924.
- 19 L. Zhang, X. Xie, H. Wang, L. Ji, Y. Zhang, H. Chen, T. Li, Y. Luo, G. Cui and X. Sun, *Chem. Commun.*, 2019, **55**, 4627–4630.
- 20 B. Li, X. Zhu, J. Wang, R. Xing, Q. Liu, X. Shi, Y. Luo, S. Liu, X. Niu and X. Sun, *Chem. Commun.*, 2020, **56**, 1074–1077.
- 21 L. Ji, X. Shi, A. M. Asiri, B. Zheng and X. Sun, *Inorg. Chem.*, 2018, **57**, 14692–14697.
- 22 L. Yang, T. Wu, R. Zhang, H. Zhou, L. Xia, X. Shi, H. Zheng, Y. Zhang and X. Sun,

- Nanoscale*, 2019, **11**, 1555–1562.
- 23 R. Zhang, L. Ji, W. Kong, H. Wang, R. Zhao, H. Chen, T. Li, B. Li, Y. Luo and X. Sun, *Chem. Commun.*, 2019, **55**, 5263–5266.
- 24 Y. Chen, B. Wu, B. Sun, N. Wang, W. Hu and S. Komarneni, *ACS Sustainable Chem. Eng.*, 2019, **7**, 18874–18883.
- 25 C. Lv, C. Yan, G. Chen, Y. Ding, J. Sun, Y. Zhou and G. Yu, *Angew. Chem., Int. Ed.*, 2018, **57**, 6073–6073.